Acta Biomaterialia 8 (2012) 218–224

Contents lists available at SciVerse ScienceDirect

Acta Biomaterialia

journal homepage: www.elsevier.com/locate/actabiomat

Mechanical testing of electrospun PCL fibers

F. Croisier [a], A.-S. Duwez [b], C. Jérôme [a,*], A.F. Léonard [c], K.O. van der Werf [d], P.J. Dijkstra [e], M.L. Bennink [d,*]

[a] Center for Education and Research on Macromolecules (CERM), Department of Chemistry, University of Liège, Sart Tilman, B6a, 4000 Liège, Belgium
[b] Nanochemistry and Molecular Systems, Department of Chemistry, University of Liège, Sart Tilman, B6a, 4000 Liège, Belgium
[c] Laboratoire de Génie Chimique, Department of Engineering, University of Liège, Sart Tilman, B6a, 4000 Liège, Belgium
[d] Nanobiophysics, Department of Science and Technology, MESA+ Institute for Nanotechnology, University of Twente, P.O. Box 217, 7500 AE Enschede, The Netherlands
[e] Polymer Chemistry and Biomaterials, Department of Science and Technology, Institute for Biomedical Technology, University of Twente, P.O. Box 217, 7500 AE Enschede, The Netherlands

ARTICLE INFO

Article history:
Received 14 April 2011
Received in revised form 7 July 2011
Accepted 16 August 2011
Available online 22 August 2011

Keywords:
Poly epsilon-caprolactone
Single fiber
Electrospinning
AFM
Mechanical properties

ABSTRACT

Poly(ε-caprolactone) (PCL) fibers ranging from 250 to 700 nm in diameter were produced by electrospinning a polymer tetrahydrofuran/*N*,*N*-dimethylformamide solution. The mechanical properties of the fibrous scaffolds and individual fibers were measured by different methods. The Young's moduli of the scaffolds were determined using macro-tensile testing equipment, whereas single fibers were mechanically tested using a nanoscale three-point bending method, based on atomic force microscopy and force spectroscopy analyses. The modulus obtained by tensile-testing eight different fiber scaffolds was 3.8 ± 0.8 MPa. Assuming that PCL fibers can be described by the bending model of isotropic materials, a Young's modulus of 3.7 ± 0.7 GPa was determined for single fibers. The difference of three orders of magnitude observed in the moduli of fiber scaffolds vs. single fibers can be explained by the lacunar and random structure of the scaffolds.

1. Introduction

Aliphatic polyesters such as poly(ε-caprolactone) (PCL), poly(lactide)s, poly(glycolide) and their copolymers are well-known materials, extensively investigated for biomedical and pharmaceutical applications. These polymers are hydrolytically and enzymatically degraded in a physiological environment into non-toxic products, which make them outstanding candidates for short- to medium-term applications [1–3]. These biomaterials are biocompatible [4–7] and may be applied in the field of tissue engineering or tissue regeneration as scaffold materials. In this respect especially, nano-sized fibers are highly interesting in that they may mimic the function of collagen fibrils in the extracellular matrix. Assemblies of nanometer-sized fibers, which can be prepared by electrospinning of polymeric solutions, are potential scaffolds which can be applied as a temporary artificial extracellular matrix [8].

A prerequisite to the use of electrospun nanofibrous scaffolds in biomedical applications is their adequate mechanical properties. Indeed, the strength and deformability of nanofibers have been demonstrated to influence in vitro cell migration, proliferation and differentiation, along with cell morphology [9–11].

The structural integrity and the mechanical strength of the scaffold are thus very important in the formation of the new tissue [12]. In this regard, the mechanical properties of both the nanofibrous scaffold and its constituent fibers are relevant in the intended application of the material for tissue regeneration.

Non-woven nanofibrous scaffolds can be tested by common macro-tensile techniques [13–16]. However, the mechanical testing of fibers with diameters <1 μm using conventional measurement methods is not possible. This requires alternative technologies able to handle individual fibers and to measure nanometer-sized deformation and forces with nN accuracy. Techniques that circumvent the aforementioned difficulties are, on the one hand, the micro- and nano-tensile testing systems [11,17,18] and, on the other hand, methods based on force microscopy measurements.

Atomic force microscopy (AFM) has proved to be a powerful tool for determining the morphology of nanometer-sized structures. This technique can also be used for the mechanical characterization of individual fibers when used in force spectroscopy mode [19]. In this respect, AFM-based nanoindentation has been increasingly applied for this purpose [15,20,21]. In this method, a sharp probe tip is pressed into a sample with a known load (force) and retracted sequentially, which generates a force–displacement curve [22]. Fitting the data with appropriate indentation models such as those proposed by Hertz [22,23], enables one to determine the elastic modulus of the fiber.

In recent years, the micro-manipulation capabilities of the AFM combined with its force–measurement efficacy were used to evaluate the response of single type I collagen fibrils with diameters ranging from 100 to 500 nm [24,25]. The Young's modulus of these

* Corresponding authors.
E-mail addresses: c.jerome@ulg.ac.be (C. Jérôme), m.l.bennink@utwente.nl (M.L. Bennink).

1742-7061/$ - see front matter © 2011 Acta Materialia Inc. Published by Elsevier Ltd. All rights reserved.
doi:10.1016/j.actbio.2011.08.015

fibrils ranges from 2 to 7 GPa in the dry state (0.2 to 0.8 GPa in the wet state; phosphate buffered saline buffer), and these values resemble those of collagen fibers present in tissues.

Although successful, the tensile testing technique employed for these fibers is relatively elaborate. Therefore, a novel method was recently developed to assess the mechanical properties of single fibers by a three-point bending technique. In this approach, an individual fiber is suspended over a micro-fabricated channel (usually in glass, polydimethylsiloxane or silicon [26–30]), and a tipless cantilever is used to bend the fiber at the center of its suspended length.

In the present study, macro- and micro-mechanical measurements techniques were applied to scaffolds and individual PCL fibers, respectively, that had been produced by electrospinning [8,31]. Fiber diameters were typically a few hundred nanometers. By conventional macro-tensile measurements using an Instron tensile testing machine, the mechanical properties of the electrospun fiber scaffolds which can be used in tissue engineering applications were determined. The mechanical properties of individual PCL fibers (as these are important for the cellular behavior in a tissue engineering application) were obtained using an AFM-based nano-scale three-point bending technique. The advantages and complementarities of these techniques are discussed with regard to their applicability to other fibrous systems.

2. Materials and methods

2.1. Preparation of PCL fibers by electrospinning

PCL with a molecular weight of 80,000 g mol^{-1} was purchased from Sigma Aldrich (USA). PCL was dissolved in 1:1 tetrahydrofurane (THF)/*N*,*N*-dimethylformamide (DMF) (w/w) at a concentration of 15 wt.%. The electrospinning process was conducted as follows: the polymer solution was transferred into a 5 ml glass syringe (Fortuna Optima with Luer-lock tip, Poulten & Graf, Wertheim, Germany) with an orthogonally cut-ended needle (G 21 1½ in., K51 Luer-lock, Italy). A syringe driver (Kd Scientific, Massachusetts, USA) was used to control the solution flow rate at 1 ml h^{-1}. To produce PCL fibers, a voltage of 12 kV was applied between the syringe needle and the collector (Series FC, Glassman High Voltage, Inc., NJ, USA). Fibers were collected on a grounded piece of aluminum foil (16 × 16 cm) which was placed on the collector plate 18 cm from the needle-end. The electrospinning set-up is schematically depicted in Fig. 1a. Platinum coating was applied to the fibers for scanning electron microscopy analysis (SEM; Jeol JSM-840A, Tokyo, Japan).

2.2. Macro-tensile measurement on PCL fiber scaffolds

Electrospinning of the PCL solution for 25 min afforded fiber scaffolds which for further analysis were cut with scissors into 3 × 0.5 cm rectangular samples, following a cardboard pattern of the same dimensions. Sample thickness was measured with a Kafer Mechanical Thickness Gauge. The porosity of the fibrous scaffold was thus not taken into account during tensile measurements, but later on. Conventional macro-tensile measurements were performed using an electromechanical tensile tester (Instron 5566, Elancourt, France). All samples were mounted between holders at a distance of 1 cm (Pneumatic Action grips, Elancourt, France). Tensile testing was conducted at a rate of 5 mm min^{-1} at room temperature (21 °C). Young's modulus (in MPa) and strain at break (%) were automatically calculated by the Instron software (Bluehill 2, Elancourt, France). To obtain Young's modulus, the software calculates the slope of each stress–strain curve in its elastic deformation region (the elastic deformation region of each curve was manually delimitated by moving cursors). Photographs of the experimental set-up are shown in Fig. 1b and c.

The porosity of PCL fiber scaffolds was estimated by combining mercury pycnometry and mercury porosimetry. Mercury (Hg) pycnometry was used to determine the apparent density of PCL fiber scaffolds. This technique allows the determination of the volume of a given mass of sample. It is based on weight differences between a calibrated cell totally filled with Hg and the same cell containing the sample, completed with mercury. Hg porosimetry (Thermo Scientific Pascal 140 and 240) was used to determine average pore size as well as the percentage of porosity (by volume) of PCL fiber scaffolds. This technique is based on the measurement of the volume of Hg intruded in the sample (the sample was placed under vacuum at ambient temperature prior to the analysis) upon application of a pressure ramp up to 200 MPa. According to the Washburn equation [32], the pressure necessary for mercury intrusion is inversely related to the pore size. The graph representing the cumulative volume of Hg intruded as a function of applied pressure gives an intrusion curve from which a pore size distribution can be calculated. In addition to the average pore size, the pore volume was determined and, knowing the apparent density of PCL fiber scaffolds, the percentage of porosity was calculated.

2.3. Three-point bending measurement on single PCL fibers

Glass substrates with parallel micro-channels were prepared using a reactive ion etching system (Electrotech Twin PF 340, Bristol, UK). The glass surface (next to the channels), owing to its high elastic modulus, was used to calibrate the deflection sensitivity of

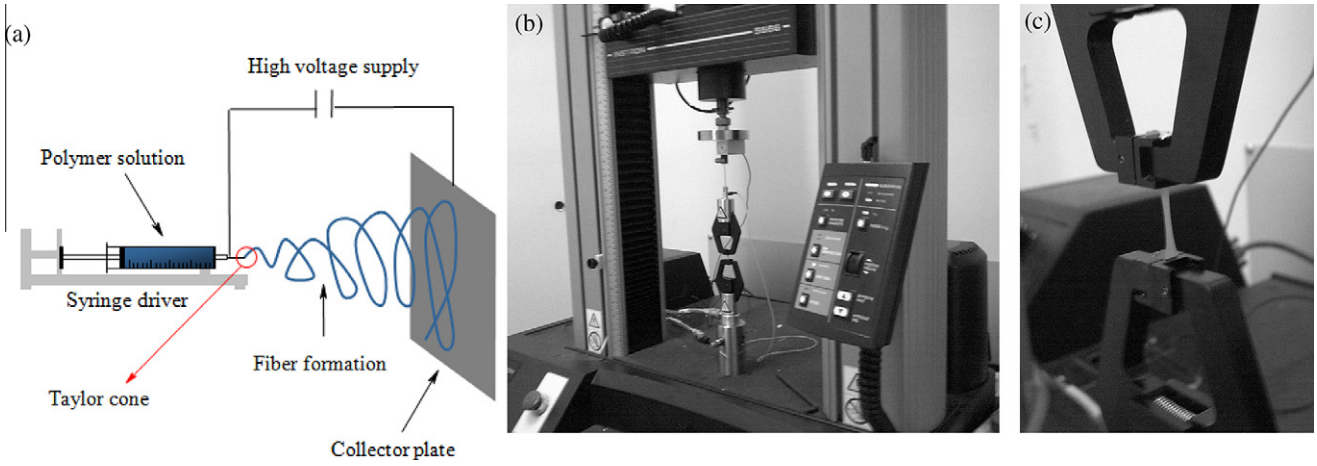

Fig. 1. (a) Schematic representation of the electrospinning set-up. (b) and (c) Photographs of the Instron experimental set-up.

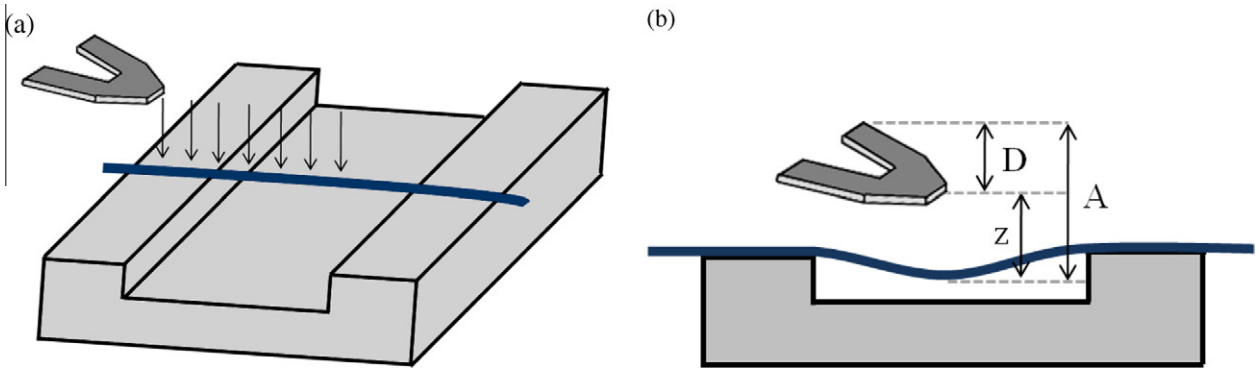

Fig. 2. (a) Schematic representation of bending experiment on a PCL electrospun fiber crossing a micrometer-sized glass channel. Deflection vs. piezo displacement curves are recorded in multiple points along the fiber. (b) Schematic representation of the distance (z), the piezo displacement (*A*) and the deflection of the AFM cantilever beam (*D*).

the AFM system. The width (7 or 10 μm) and depth (450 nm) of the channels were determined by high-resolution SEM (HR-SEM; LEO 1550, Carl Zeiss, Munich, Germany) measurements. Electrospun PCL fibers were extracted from electrospun scaffolds (aluminum foil) by gently pressing the glass substrates directly on the electrospun foil. The presence of fibers on the glass substrate was then confirmed by optical microscopy. Si tips (NSC36/Cr–Au, MikroMasch, San Jose, CA, USA) were used for imaging the topography of the PCL fibers. Modified triangular silicon nitride cantilevers (coated sharp microlevers MSCT-AUHW, type F, spring constant $k = 0.5\ \mathrm{N\ m^{-1}}$, Veeco, Cambridge, UK) were used in the bending tests. The tip on the AFM cantilever was removed using a focused ion beam (FIB; Nova NanoLab 600, FEI Company, Eindhoven, The Netherlands) to avoid damage to the fiber surface during the bending measurements and to reduce the amount of indentation into the fibrous material. The spring constant of the FIB-treated cantilever was calibrated ($1\ \mathrm{N\ m^{-1}}$) using the thermal tune method (Veeco).

By means of an optical microscope coupled to a commercial AFM (Bioscope II and Nanoscope V, Veeco, Cambridge, UK), individual PCL fibers suspended over the channels were selected and employed in the bending measurements. Deflection vs. piezo displacement curves were recorded at different positions along the fiber suspended across the channel, as depicted in Fig. 2. The AFM cantilever was displaced over a range of 1–3 μm at a frequency of 1.03 Hz in the bending tests.

3. Results and discussion

3.1. Preparation of PCL fibers by electrospinning

PCL fibers and non-woven fiber scaffolds were produced by electrospinning [31]. A solution with the appropriate viscosity for electrospinning was made by dissolving PCL with a molecular weight of 80,000 $\mathrm{g\ mol^{-1}}$ in a THF/DMF mixture (1:1 w/w). The electrospinning conditions were optimized (solution containing 15% by weight of PCL, applied voltage 12 kV, distance 18 cm and flow rate $1\ \mathrm{ml\ h^{-1}}$) in order to obtain continuous fibers exempt of beads or other defects with diameters <1 μm, as these are well-suited for application in biomedical scaffolds [8]. The resulting PCL fibers had a smooth surface free of any beaded defects.

Representative SEM images of PCL electrospun fibers collected on aluminum foil are presented in Fig. 3. The diameters of the fibers as measured from the images range from 250 to 700 nm.

3.2. Macro-tensile measurement on PCL fiber scaffolds

PCL fibers scaffolds were mounted in the Instron tensile tester and stretched in order to determine their Young's modulus and strain at break. Eight different samples were tested. The results are reported in Table 1, and the stress–strain curves are presented in Fig. 4. The mean value of the Young's modulus was 3.8 ± 0.8 MPa, and the average value of strain at break was 170 ± 10%. These values are consistent with those reported in literature for non-woven and oriented PCL fiber scaffolds composed of fibers with a similar diameter range [15,16].

In comparison, the Young's modulus of extruded PCL films (with molecular weight 80,000 $\mathrm{g\ mol^{-1}}$), determined by macro-tensile testing (Instron), is 190 ± 6 MPa [33].

The differences between the Young's modulus of PCL fiber scaffolds and that of extruded films might originate from the porosity of fiber scaffolds, interactions between fibers (slip of fibers over one another, point bonding, crosslinking) and fiber orientation [13,34,35].

SEM images (Fig. 3) show no particular orientation of the fibers (random fibers) and no noticeable point bonding—though this does

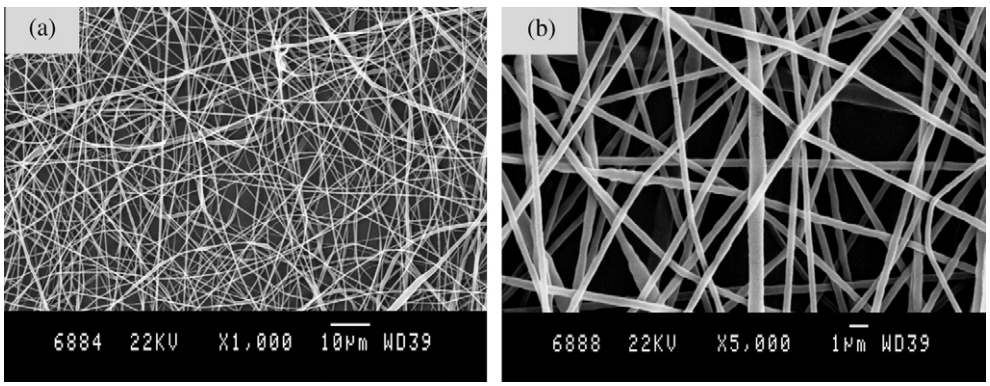

Fig. 3. SEM images of PCL electrospun fibers collected on aluminum foil and metal coated with Pt before analysis.

Table 1
Results of Instron macro-tensile testing on PCL fibers scaffolds (Note: The standard deviation in the modulus is 0.8 MPa and in the strain at break 10%).

PCL fibers sample	Young's modulus (MPa)	Strain at break (%)
1	5.200	170
2	4.100	170
3	3.100	170
4	3.200	190
5	4.500	170
6	3.700	170
7	2.900	180
8	3.700	160

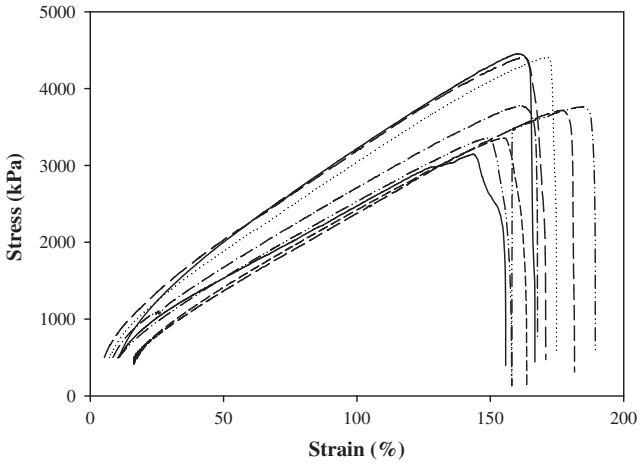

Fig. 4. Stress–strain curves obtained for eight different samples of PCL electrospun fiber mats.

not prove that it does not exist within the fiber mat. Moreover, no preliminary crosslinking of the fibers was realized. The differences between the mechanical properties of fiber scaffolds and films are thus most likely due to porosity. In fact, fiber scaffolds prepared by electrospinning present a high percentage of porosity. It typically ranges from 70% to 90% (v/v) [36]. Mercury pycnometry and porosimetry were used to determine the porosity of the PCL fiber scaffolds. By the pycnometry technique, an apparent density of 0.349 ± 0.001 g cm^{-3} was calculated for PCL fiber scaffolds. Average pore size was determined by Hg porosimetry and was equal to 1300 ± 500 nm. However, this value should be considered with caution, as it was calculated using the Washburn model under the approximation of cylindrical pores that are hardly interconnected [32,37]. The calculated percentage of porosity (v/v) of PCL fiber scaffolds is $87.1 \pm 4.4\%$ v/v, which corresponds to the value reported in the literature [36].

This extremely high percentage of porosity could certainly explain the lower Young's modulus obtained for PCL fiber scaffolds. A quantitative relationship between the porosity of the sample and its Young's modulus would require a more detailed study, with samples of various porosities.

Nevertheless, the Young's modulus measured on the fiber scaffolds remains relevant, to judge from the interest in the potential biomedical applications of such constructs, as they predict the mechanical response of non-woven scaffolds in contact with adjacent tissues; varying the sample porosity might be a way to adjust the mechanical resistance of the scaffold.

The mechanical properties of single nanofibers within the scaffolds are also important in the understanding of the behavior of cells that will attach to the fiber as they are developing new tissue. A technique to determine the mechanical properties of the single electrospun fibers is described in the following section.

3.3. Three-point bending measurement on single PCL fibers

Individual PCL fibers perpendicularly spanning the micro-fabricated channels were selected using an optical microscope integrated with an AFM microscope. The AFM topography image of such a PCL fiber using a Si tip is shown in Fig. 5a and b. For the bending test, this tip was replaced by a tipless cantilever to prevent local indentation of the fiber. Bending was conducted at different positions along the fiber and the glass substrate, as depicted in Fig. 2.

Using commercial AFM software (Nanoscope, Veeco), 100 deflection–piezo displacement curves were recorded along the suspended fiber, including the parts where it was supported by the glass rims. It is important to mention that no difference was found in the deflection–piezo displacement curves recorded when bending was performed at the same position several times, which indicates that no permanent deformation of the fiber occurred during the bending test.

Force–distance (F–z) curves for every bending experiment were calculated from the deflection–piezo displacement curves using the following equations [29]:

$$Z = A - D \tag{1}$$

$$F = D \times k \tag{2}$$

in which A is the piezo displacement, D the deflection of the AFM cantilever beam, and k is the spring constant of the cantilever. Parameters A, D and z are schematized in Fig. 2b.

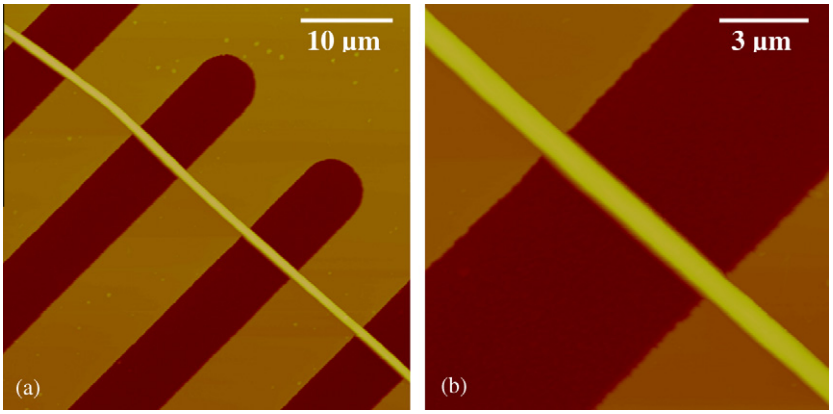

Fig. 5. (a) and (b) AFM height images of a PCL electrospun fiber perpendicularly suspended over glass channels (two different magnifications).

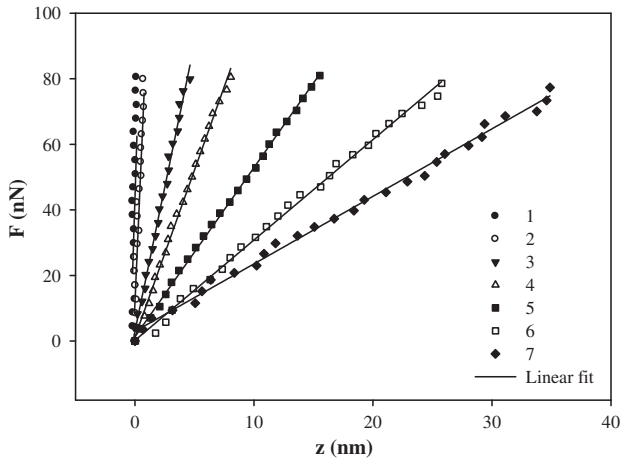

Fig. 6. *F–z* curves (repulsive part) obtained at different positions along a suspended PCL fiber (radius = 210 nm). The index of each curve refers to a particular bending position, as shown in Figs. 2 and 7. Curve 1 was recorded on the glass surface, curve 2 on the PCL fiber deposited on the glass surface, curve 3 on the fiber at the edge of the glass channel, curves 4–6 on the fiber between the edge and the middle of the channel, and curve 7 on the fiber at the mid-point of its suspended length.

Seven *F–z* curves are presented in Fig. 6. Only the part of the curves in which the tip is in contact with the fiber is depicted. The slope (d*F*/d*z*) of each force–distance curve was determined by a linear curve-fit of this part of the curves. No significant slope difference was found when curves were recorded directly on the glass substrate (Fig. 6, curve 1) or on a PCL fiber deposited on this glass surface (Fig. 6, curve 2).

However, a decrease in the slope of the *F–z* curves was observed when the suspended part of the fiber was recorded as result of the bending (Fig. 6, curves 3–7). As expected, a minimum in the slope—which corresponds to the largest bending amplitude—is found for the fiber portion located at the center of the channel (Fig. 6, curve 7).

Fig. 7 is a figure showing the slope of the *F–z* curves as a function of the position on the fiber where the bending was performed.

Profiles similar to that presented in Fig. 7 have been observed for 12 different PCL fibers. Three of them, being perpendicular to more than one channel (as illustrated in Fig. 5a), could be measured at several locations.

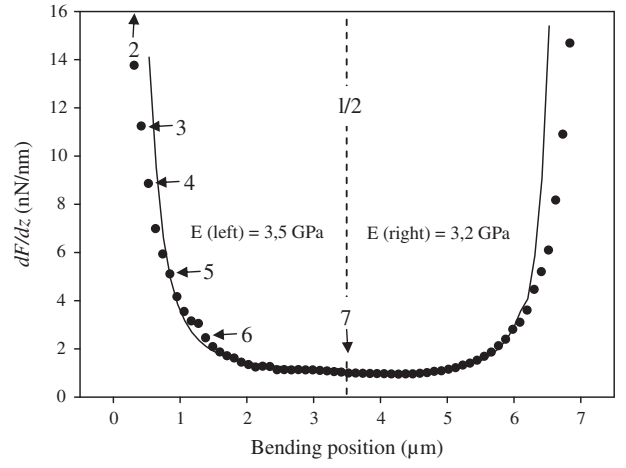

Fig. 7. Slope (d*F*/d*z*) of the *F–z* curves obtained for a PCL electrospun fiber (radius = 210 nm) as a function of the bending position of the fiber along the channel (channel width = 7 µm). The dashed line on the graph shows the middle point of the channel (l/2). Numbered arrows represent a particular bending position, corresponding to *F–z* curves depicted in Fig. 6. The d*F*/d*z* data on the left and on the right half of the channel are fitted separately to Eq. (4). The error in the fitting is ~6% (left half) and ~5% (right half).

The gradient (d*F*/d*z*) of the force–distance curve, obtained from bending the suspended fiber at its mid-point, was plotted as a function of the radius of the PCL fiber (Fig. 8). The diameters of all fibers were determined by HR-SEM measurements. As expected, the effective spring constant (d*F*/d*z*) appears to increase with the radius of the tested fibers.

The fiber bending modulus was derived from force–distance curves according to the following expression [38]:

$$E = \frac{l^3}{1921} \times \frac{dF}{dz} \tag{3}$$

in which *I* is the surface moment of inertia and is equal to ¼πR^4 (the fiber is considered as a rod with a circular cross-section of radius *R*), *l* is the length of the PCL electrospun fiber suspended across the channel, and d*F*/d*z* is the slope of the force–distance curve obtained from bending the mid-point of the PCL fiber spanning the channel.

During imaging [39] (with various angles between fiber axis and fast scan direction) and during the bending tests, the PCL fibers did not show any movement. The interactions between the PCL fiber and the glass surface are expected to be able to withstand the forces applied to it by bending. This implies that Eq. (3) (corresponding to a clamped beam bending model [39]) could be used in the calculation of the bending modulus of the PCL fibers.

The mean value obtained for PCL electrospun fibers was 3.7 ± 0.7 GPa. The bending modulus as a function of the PCL fiber radius is illustrated in Fig. 9.

The bending modulus of the PCL fibers can also be obtained by fitting the measured slope of the force–distance (*F–z*) curves at all bending positions to Eq. (4) [38]:

$$\frac{dF}{dz} = \frac{3 \times l^3 \times E \times I}{(1-x)^3 \times x^3} \tag{4}$$

in which d*F*/d*z* is the slope of the force–distance curve, *l* is the length of the PCL electrospun fiber suspended across the channel, *E* is the bending modulus, *I* is the surface moment of inertia and is equal to ¼πR^4 (the fiber is considered as a rod with a circular cross-section of radius *R*), and *x* is the bending position ($0 \leqslant x \leqslant l$).

Fig. 7 shows that the d*F*/d*z* data fit Eq. (4). Two different fits were realized, on the left and on the right half of the fiber. Similar results to those obtained via Eq. (3). are achieved.

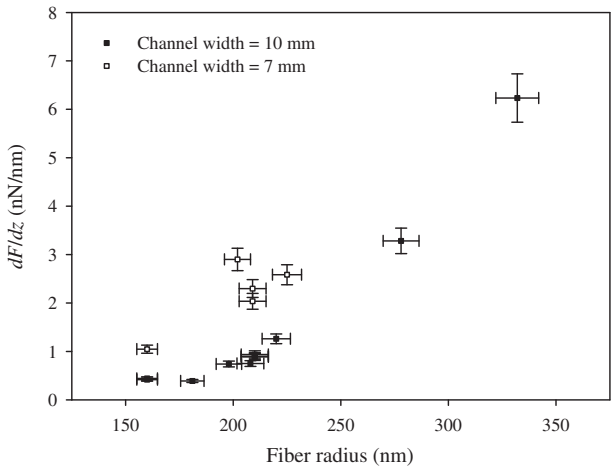

Fig. 8. Slope (d*F*/d*z*) of the *F–z* curves, obtained from bending the middle point of suspended PCL electrospun fibers, as a function of the radius of the fibers. The error bars in the figure are derived from the errors in fiber radius (due to the accuracy of HR-SEM measurements) (~3%), the spring constant of the cantilever (~5%) and the fitting (~3%).

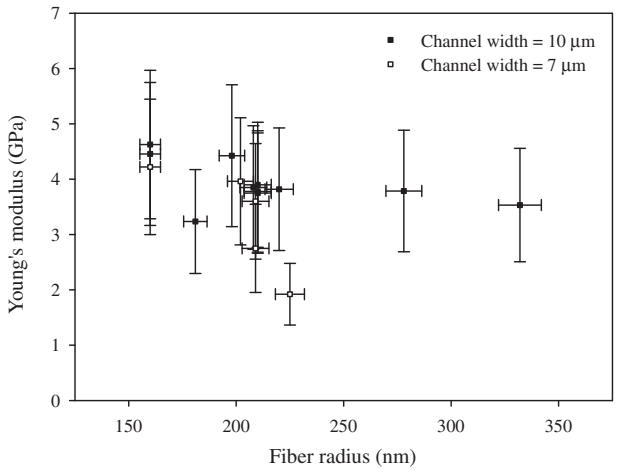

Fig. 9. Bending modulus of PCL electrospun fibers as a function of the fiber radius, obtained from bending mid-point of suspended fiber. The error bars in the figure are derived from the errors in fiber radius (~3%), the spring constant of the cantilever (~5%), the width of the channel (~3%) and the fitting (~3%).

For isotropic materials or rods with a high length-to-diameter ratio, the Young's modulus is identical to the bending modulus. Only in the case where the modulus depends on the diameter, a shear contribution in the deflection of the fiber or fibril has to be taken in account in order to calculate the Young's modulus [38]. In the present case, the suspended length of PCL electrospun fibers is ~10 μm, whereas the fiber diameter ranges from 250 to 700 nm. Moreover, the bending modulus does not seem to be influenced by the fiber radius—at least for the measured range—as illustrated in Fig. 9. The Young's modulus is therefore taken as equal to the obtained bending modulus.

The macro-tensile measurements performed on PCL fiber scaffolds lead to a Young's modulus of 3.8 ± 0.8 MPa. The Young's modulus found for the individual PCL fibers was only 3.7 ± 0.7 GPa, which is three orders of magnitude higher. This difference can be explained by the lacunar structure (high porosity) of the fiber scaffolds and the random orientation of its constituting fibers [15]. Both Young's moduli are very relevant, as they provide information on mechanical properties either at tissue or cellular scale.

4. Conclusions

Two approaches are reported for the evaluation of fiber mechanical properties. To the authors' knowledge, this is the first study applying a nanoscale three-point bending method to PCL electrospun fibers. This AFM-based technique is versatile and might now be applied to other fiber types.

Acknowledgments

F.C. is grateful to the Belgian "Fonds pour la Formation à la Recherche dans l'Industrie et dans l'Agriculture" (FRIA) for financial support. This work was supported by the Science Policy Office of the Belgian Federal Government (IAP 6/27). CERM thanks J.P. Pirard and C. Bodson from the "Laboratoire de Génie Chimique" (ULg) for the porosity measurements (IAP 17/6).

Appendix A. Figures with essential colour discrimination

Certain figures in this article, particularly Figures 1, 2 and 5, are difficult to interpret in black and white. The full colour images can be found in the on-line version, at doi:10.1016/j.actbio.2011.08.015).

References

[1] Albertsson A-C, Varma IK. Aliphatic polyesters: synthesis, properties and applications. Adv Polym Sci 2002;157:1–40.
[2] Smith R. Biodegradable polymers for industrial applications. Cambridge: Woodhead; 2005.
[3] Rabetafika HN, Paquot M, Dubois P. Features of plant-based polymers with special applications in plastic field. Biotechnol, Agronom, Soc Environ 2006;10:185–96.
[4] Vert M. Bioresorbable synthetic polymers and their operation field. In: Walenkamp G, editor. Stutgart: Georg Thieme; 1998.
[5] Jerome C, Lecomte P. Recent advances in the synthesis of aliphatic polyesters by ring-opening polymerization. Adv Drug Deliv Rev 2008;60:1056–76.
[6] Vert M, Li SM, Spenlehauer G, Guerin P. Bioresorbability and biocompatibility of aliphatic polyesters. J Mater Sci Mater Med 1992;3:432–46.
[7] Sun H, Mei L, Song C, Cui X, Wang P. The in vivo degradation, absorption and excretion of PCL-based implant. Biomaterials 2006;27:1735–40.
[8] Ramakrishna S, Fujihara K, Teo WE, Lim CT, Ma Z. An introduction to electrospinning and nanofibers. Singapore: World Scientific; 2005. p. 396.
[9] Zhang Y, Lim CT, Ramakrishna S, Huang Z-M. Recent development of polymer nanofibers for biomedical and biotechnological applications. J Mater Sci Mater Med 2005;16:933–46.
[10] Carnegie JA, Cabaca O. Extracellular matrix composition and resilience. Two parameters that influence the in vitro migration and morphology of rat inner cell mass-derived cells. Biol Reprod 1993;48:287–99.
[11] Tan EPS, Ng SY, Lim CT. Tensile testing of a single ultrafine polymeric fiber. Biomaterials 2005;26:1453–6.
[12] Tan EPS, Goh CN, Sow CH, Lim CT. Tensile test of a single nanofiber using an atomic force microscope tip. Appl Phys Lett 2005;86. 073115/1-/3.
[13] Kim GH, Han H, Park JH, Kim WD. An applicable electrospinning process for fabricating a mechanically improved nanofiber mat. Polym Eng Sci 2007;47:707–12.
[14] Lee KH, Kim HY, Khil MS, Ra YM, Lee DR. Characterization of nano-structured poly(ε-caprolactone) nonwoven mats via electrospinning. Polymer 2003;44:1287–94.
[15] Thomas V, Jose MV, Chowdhury S, Sullivan JF, Dean DR, Vohra YK. Mechano-morphological studies of aligned nanofibrous scaffolds of polycaprolactone fabricated by electrospinning. J Biomater Sci, Polym Ed 2006;17:969–84.
[16] Bolgen N, Menceloglu YZ, Acatay K, Vargel I, Piskin E. In vitro and in vivo degradation of nonwoven materials made of poly(ε-caprolactone) nanofibers prepared by electrospinning under different conditions. J Biomater Sci, Polym Ed 2005;16:1537–55.
[17] Wong S-C, Baji A, Leng S. Effect of fiber diameter on tensile properties of electrospun poly(vepsiln-caprolactone). Polymer 2008;49:4713–22.
[18] Lim CT, Tan EPS, Ng SY. Effects of crystalline morphology on the tensile properties of electrospun polymer nanofibers. Appl Phys Lett 2008;92. 141908/1-/3.
[19] Tan EPS, Lim CT. Mechanical characterization of nanofibers—A review. Compos Sci Technol 2006;66:1102–11.
[20] Vondran JL, Sun W, Schauer CL. Crosslinked, electrospun chitosan-poly(ethylene oxide) nanofiber mats. J Appl Polym Sci 2008;109:968–75.
[21] Tan EPS, Lim CT. Nanoindentation study of nanofibers. Appl Phys Lett 2005;87. 123106/1-/3.
[22] Jee A-Y, Lee M. Comparative analysis on the nanoindentation of polymers using atomic force microscopy. Polym Testing 2009;29:95–9.
[23] Hertz HJ. On the contact of rigid elastic solids and hardness. J Reine Angew Math 1881;92:156–71.
[24] van der Rijt JAJ, van der Werf KO, Bennink ML, Dijkstra PJ, Feijen J. Micromechanical testing of individual collagen fibrils. Macromol Biosci 2006;6:697–702.
[25] van der Rijt JAJ. Micromechanical testing of single collagen type I fibrils, PhD thesis, University of Twente, Enschede, The Netherlands; 2004.
[26] Tan EPS, Lim CT. Physical properties of a single polymeric nanofiber. Appl Phys Lett 2004;84:1603–5.
[27] Tan EPS, Lim CT. Effects of annealing on the structural and mechanical properties of electro-spun polymeric nanofibres. Nanotechnology 2006;17:2649–54.
[28] Yang L, van der Werf KO, Koopman BFJM, Subramaniam V, Bennink ML, Dijkstra PJ, et al. Micromechanical bending of single collagen fibrils using atomic force microscopy. J Biomed Mater Res A 2007;82A:160–8.
[29] Yang L, Fitie CFC, van der Werf KO, Bennink ML, Dijkstra PJ, Feijen J. Mechanical properties of single electrospun collagen type I fibers. Biomaterials 2008;29:955–62.
[30] Yang L, van der Werf KO, Fitie CFC, Bennink ML, Dijkstra PJ, Feijen J. Mechanical properties of native and cross-linked type I collagen fibrils. Biophys J 2008;94:2204–11.
[31] Formhals A. Artificial threads. Application. US: Schreiber-Gastell, Richard; 1940.
[32] Washburn EW. Note on a method of determining the distribution of pore sizes in a porous material. Proc Natl Acad Sci USA 1921;7:115–6.
[33] Averous L, Moro L, Dole P, Fringant C. Properties of thermoplastic blends: starch-polycaprolactone. Polymer 2000;41:4157–67.

[34] Wang M, Jin H-J, Kaplan DL, Rutledge GC. Mechanical properties of electrospun silk fibers. Macromolecules 2004;37:6856–64.
[35] Lee KH, Kim HY, Ryu YJ, Kim KW, Choi SW. Mechanical behavior of electro spun fiber mats of poly(vinyl chloride)/polyurethane polyblends. J Polym Sci, B: Polym Phys 2003;41:1256–62.
[36] Lowery JL. Characterization and modification of porosity in electrospun polymeric materials for tissue engineering applications. Massachusetts: Massachusetts Institute of Technology; 2009.
[37] Anon. Handbook of sol-gel science and technology: processing, characterization and applications, vol. II. In: Pirard R, Alié C, Pirard JP, editors. Specific behavior of sol gel materials in mercury porosimetry: collapse and intrusion. In: Sumio Sakka (Professor Emeritus of Kyoto University), editor. Boston, Dordrecht, London: Kluwer Academic Publishers; 2005.
[38] Gere JM, Timoshenko SP. Mechanics of materials. 4th ed. Cheltenham: Stanley Thornes; 1999.
[39] Cuenot S, Demoustier-Champagne S, Nysten B. Elastic modulus of polypyrrole nanotubes. Phys Rev Lett 2000;85:1690–3.